Chemical Engineering Journal 160 (2010) 333–339

Contents lists available at ScienceDirect

Chemical Engineering Journal

journal homepage: www.elsevier.com/locate/cej

Autothermal reforming of ethanol for hydrogen production over perovskite $LaNiO_3$

Hongqing Chen[a], Hao Yu[a,*], Feng Peng[a,*], Guangxing Yang[a], Hongjuan Wang[a], Jian Yang[a], Yong Tang[b]

[a] School of Chemistry and Chemical Engineering, South China University of Technology, Guangzhou 510640, People's Republic of China
[b] School of Mechanical Engineering, South China University of Technology, Guangzhou 510640, People's Republic of China

ARTICLE INFO

Article history:
Received 29 December 2009
Received in revised form 14 March 2010
Accepted 20 March 2010

Keywords:
Hydrogen production
Autothermal reforming
Ethanol
Perovskite
Ni/La_2O_3
Dispersion
Coking

ABSTRACT

$LaMnO_3$, $LaFeO_3$, $LaCoO_3$ and $LaNiO_3$ perovskite oxides were prepared using combustion method for autothermal reforming of ethanol (ATRE). Fresh, reduced and used catalysts were characterized by XRD, TEM, ethanol-TPD, and H_2-TPR. The perovskite-type oxides exhibit moderate activities in the ATRE reaction. Well dispersed Ni particles on lanthanum oxide species were obtained by reducing the $LaNiO_3$ sample. It favors the dehydrogenation, decomposition of ethanol/acetaldehyde, methane reforming and water gas shift reactions, thus leads to good activity and H_2 selectivity in ATRE reaction. Typically, 3.2 H_2 molecules per ethanol molecule were produced at $EtOH:H_2O:O_2 = 1:2:0.98$ and $GHSV = 4 \times 10^5\ h^{-1}$. A comparison between $LaNiO_3$ derived and impregnated Ni/La_2O_3 shows that the $LaNiO_3$ derived sample favored the dispersion of Ni, which increased the activity and the resistance to coke deposition.

1. Introduction

Autothermal reforming (ATR) process has attracted much attention because of its high efficiency for hydrogen production and less dependence on additional power sources [1–4]. Hydrocarbons or carbohydrates, such as methane, propane, diesel fuel, cellulose, ethanol, can be used as fuels for the ATR reaction for hydrogen production [1,5–9]. Since ethanol is a transportable, non-toxic and renewable energy carrier, reforming of ethanol is considered as one of the most attractive and sustainable solutions for hydrogen production in the areas of fuel cell. By co-feeding ethanol with steam and oxygen/air, hydrogen can be effectively extracted from ethanol via the oxidation and the steam reforming reactions. As shown in the following equation, with appropriate oxygen stoichiometry, the heat needed by the steam reforming reaction can be supplied by the exothermic oxidation reaction, thus no additional heat is required.

$$C_2H_5OH + (3-2\delta)H_2O + \delta O_2 \rightarrow 2CO_2 + (6-2\delta)H_2 \quad (\delta \geq 0.61, \Delta H \leq 0)$$

Noble metal catalysts, such as $Rh–Ce/Al_2O_3$ [5] and Ir/La_2O_3 [10,11], have been proved to be excellent for the autothermal reforming of ethanol (ATRE). However, the high expense of noble metal would limit their application on large scale. Base metals, represented by Ni, Co, etc., have been widely investigated for steam reforming (SR), oxidative steam reforming (OSR), partial oxidation and ATR reactions of ethanol due to their excellent C–C bond cleavage ability and low costs [12–17]. However, these catalysts are also highly active in coke deposition. To prevent coking, Ni crystallites in small size are highly desired. Kock et al. [18] have reported that the size of metallic Ni particles was a key factor for coke formation, and the critical size of Ni particles at which the coke deposition can be inhibited was suggested to be about 10 nm over SiO_2. Similar results have also been obtained in nickel catalyzed cyclopentane hydrogenolysis [19,20] and CO_2 reforming of methane [21].

The incipient wetness impregnation method has been extensively used for the preparation of Ni, Co and noble metal catalysts [22]. However, the size of the active phase obtained by this method is usually large (>20 nm), especially at high loadings (>10 wt.%) [23–25]. Perovskite oxides with general formula of ABO_3 have been investigated extensively due to their thermal stability, oxygen storage capacity and oxygen ion conductivity [26–30]. Recently, $LaNiO_3$ and M substituted $LaM_xNi_yO_3$ (M = Ce, Sr, Cr, Mn, Fe, K, Li, Co, etc.) oxide catalysts have been used in the dry reforming of methane and ATR of hydrocarbons [9,31–34]. By reducing B-site Ni cations, metal crystallites can be well dispersed over La_2O_3 oxide [8,9]. A superior catalytic performance of the perovskite-derived catalyst to the impregnated Ni/La_2O_3 has been reported by Gallego et al.

* Corresponding authors. Tel.: +86 20 8711 4916; fax: +86 20 8711 4916.
E-mail addresses: yuhao@scut.edu.cn (H. Yu), cefpeng@scut.edu.cn (F. Peng).

1385-8947/$ – see front matter © 2010 Elsevier B.V. All rights reserved.
doi:10.1016/j.cej.2010.03.054

[35] in the dry reforming of methane. However, few papers have paid attention to the application of perovskite-derived catalysts in the ATRE reaction.

In this paper, perovskite-type $LaNiO_3$, $LaCoO_3$, $LaMnO_3$ and $LaFeO_3$ oxides were synthesized to produce hydrogen via the ATRE pathway. The effect of reducibility of these oxides on the catalytic behavior in ATRE reaction was discussed. The impregnated Ni/La_2O_3 was also employed to compare the catalytic characteristic with perovskite-type $LaNiO_3$. Careful investigations of the structure of the catalysts were performed to understand the relationship between activity, stability and their structural and surface characteristics.

2. Experimental

2.1. Catalyst preparation

The $LaMO_3$ (M = Ni, Co, Fe, Mn) perovskites were synthesized by a combustion method [36]. Stoichiometric amounts of $La(NO_3)_3{\cdot}6H_2O$, $Ni(NO_3)_3{\cdot}6H_2O$, $Mn(NO_3)_3$, $Co(NO_3)_2{\cdot}6H_2O$, or $Fe(NO_3)_3{\cdot}9H_2O$ were dissolved in deionized water. Citric acid and ethylene glycol were added as complexing agents into the solution. The molar ratio of total cations, citric acid and ethylene glycol was 1:1:1. The resulted solution was heated at 120 °C overnight to remove the solvent and to form gel. Then the solids were calcined at 400 °C for 2 h and then at 700 °C for 6 h. Before the ATRE reaction, the catalysts were reduced with hydrogen of 50 ml/min at 500 °C for 40 min.

To investigate the effect of preparation method, Ni/La_2O_3 catalysts were synthesized by the incipient wetness impregnation method with an aqueous solution of nickel nitrate. The loadings of nickel were controlled at 10 and 23.9 wt.%. The latter loading corresponds to the Ni/La atom ratio of 1:1. The impregnated catalysts were dried at 120 °C overnight, and then calcined at 500 °C in air for 2 h. The samples by the impregnation method are denoted as $Ni(x)/La_2O_3$, where x is the weight percentage of Ni.

2.2. Catalyst characterization

X-ray diffraction experiments were carried out from 5° to 90° with step-size of 0.02° and counting times of 2 s (XRD, Rigaku, D/max-IIIA). Prior to analysis, the samples were cooled down to room temperature in N_2 atmosphere and sealed in a dryer with fresh silica gel. Temperature program reduction (TPR) and desorption (TPD) experiments were carried out in an Auto Chem II chemisorption Analyzer. For TPR, 0.15 g sample was firstly flushed with a nitrogen flow at 50 cm^3/min at 120 °C to remove adsorbed water, and then was reduced in a flow of H_2/Ar (10 vol.% of hydrogen) at a ramping rate of 10 °C/min. Hydrogen consumption was monitored by a thermal conductivity detector (TCD). The effluent gas was passed through a zeolite column to remove water before entering TCD. For TPD, 0.1 g sample was firstly reduced at 500 °C with 10 vol.% H_2/Ar (50 cm^3/min) for 40 min. After purging with He for 30 min, the sample was cooled down to 50 °C. The adsorption of ethanol was carried out by pulsing argon saturated by ethanol at 30 °C, and was followed by purging with He for 30 min to clean pipelines. The ethanol uptake was determined by calibrating the pulse signal from the TCD detector with the ethanol dose. Then the TPD profiles of H_2, CO, CO_2, CH_4 and EtOH (m:z = 2, 28, 44, 31, respectively) were recorded by an online mass spectrometer (QIC-20, Hiden Analytical) from 50 to 800 °C under a flow of Ar at 20 ml/min and at a ramping rate of 10 °C/min. TEM images were obtained in a JEM-2010 (JEOL) microscope operating at 200 kV equipped with an INCA Energy Dispersive Spectrometer (Oxford Instruments). Specimens for TEM were prepared by ultrasonically suspending the sample in acetone and depositing a drop of the suspension onto a TEM grid.

2.3. Catalytic reaction

The ATRE reaction was carried out in a quartz fixed-bed reactor with a preheater. The inner diameter of the micro packed-bed reactor was 8 mm. In each experiment, 55 mg catalysts were sandwiched with quartz wool and packed in the reactor. A thermocouple was inserted into the center of the catalytic bed to monitor the reaction temperature. The mixture of ethanol and water with 1:2 molar ratio was fed into the preheater by a syringe pump at a flow rate of 0.3 ml/min, and was vaporized at 240 °C. Air at room temperature was introduced and mixed with the gaseous reactant at the inlet of the reactor. The flow rate was in the range of 250–400 ml/min. Correspondingly, the molar ratio of $EtOH{:}H_2O{:}O_2$ was 1:2:0.6–2.0. The heater of reactor was turned off as soon as the catalyst reduction procedure was over. When the reactor was cooled down to 400 °C, the mixture of air/ethanol/H_2O was introduced into the reactor without any additional energy input. During the ATR reaction, the temperature varied between 500 and 700 °C according to reaction conditions and catalysts employed. The reactions were carried out at an ethanol-based weight hourly space velocity (WHSV) of 160 h^{-1}. Correspondingly, the gas space hourly velocity (GHSV) varied between 3×10^5 and 5×10^5 h^{-1} and the contact time was about 7–12 ms. The WHSV and GHSV were calculated by:

$$\mathrm{WHSV} = \frac{M_{\mathrm{Ethanol}} \times F_{\mathrm{Ethanol,\ in}}}{V \times \rho \times t}$$

$$\mathrm{GHSV} = \frac{22,400 \times F_{\mathrm{total,in}}}{V \times t}$$

where M is the molecular weight, F is the normal flow rate in mol/h, V is the volume of the catalyst bed in cm^3, ρ is the bulk density of catalyst in g/cm^3, and t is the time in hour.

The reformate was analyzed by an Agilent 6820 GC equipped with Haysep (for the analysis of CO_2, C_2H_4, ethanol, acetaldehyde, water, and acetone), 13X molecular sieve (for H_2, N_2, CO, CH_4) packed columns and TCD detector. N_2 was used as an inert standard to calculate the mass balances. The carbon balances of GC analysis were within 100 ± 10%. The ethanol conversion and product selectivities were calculated by:

$$X_{\mathrm{Ethanol}} = \frac{F_{\mathrm{Ethanol,\ in}} - F_{\mathrm{Ethanol,\ out}}}{F_{\mathrm{Ethanol,\ in}}}$$

$$S_{\mathrm{H_2}} = \frac{F_{\mathrm{H_2\ out}}}{(6-2\delta) \times F_{\mathrm{Ethanol,\ in}} \times X_{\mathrm{Ethanol}}}$$

$$S_i = \frac{m \times F_{\mathrm{i,out}}}{2 \times F_{\mathrm{Ethanol,\ in}} \times X_{\mathrm{Ethanol}}}$$

where F is the normal flow rate, m is the number of carbon atoms in a product molecule, and δ is the stoichiometric number of O_2 in the ATRE reaction.

3. Results and discussion

3.1. Characterization of perovskite-derived catalysts

XRD was used to investigate the crystallite compositions of the fresh and reduced $LaMnO_3$, $LaCoO_3$, $LaFeO_3$ and $LaNiO_3$ samples. After calcined at 700 °C, all the samples present perovskite structure (JCPDS 750440, 480123, 371493, 330711), as shown in Fig. 1(a). A group of peaks in the 2θ range of 27.5–29° were detected in $LaFeO_3$. The origin for these peaks could be attributed to diffraction peaks of other La–Fe complex oxides, which might be reduced by H_2 at 500 °C. However, the detail is not clear yet on the current stage. The diffraction peaks of perovskite structure disappeared after reducing the $LaNiO_3$ sample at 500 °C for 40 min (Fig. 1(b)), and

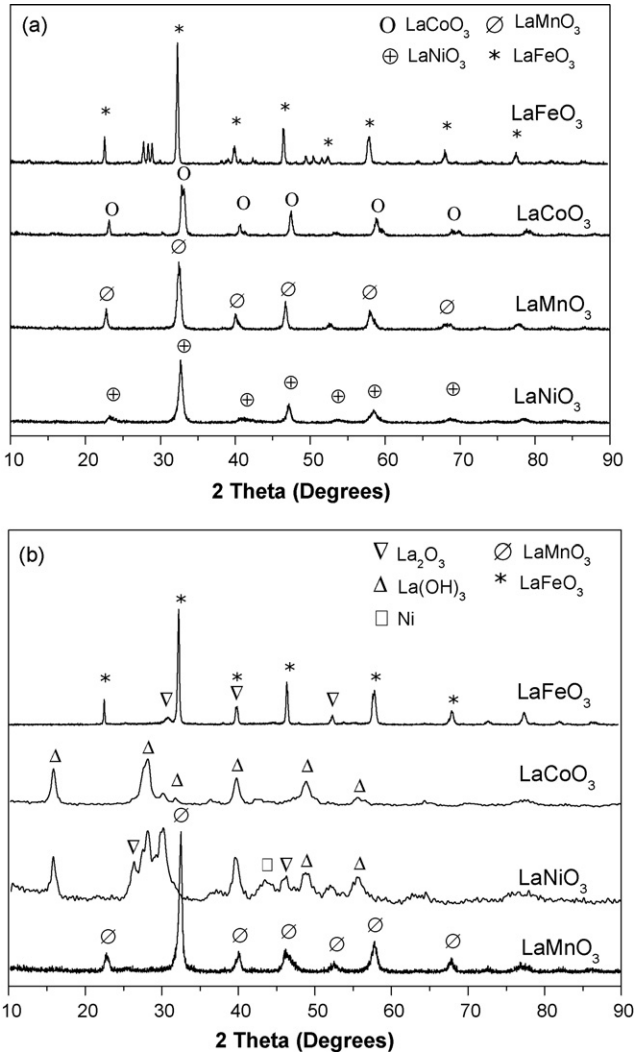

Fig. 1. XRD patterns of fresh (a) and reduced (b) $LaMnO_3$, $LaCoO_3$, $LaFeO_3$ and $LaNiO_3$ catalysts.

a group of dispersed peaks were obtained, which can be attributed to La_2O_3 (JCPDS 050602) and $La(OH)_3$ (JCPDS 361481). Ni^0 shows only a broad peak at 44.4° (JCPDS 040850). By applying Scherrer's equation using the (1 0 0) reflection, the Ni^0 crystallite size was calculated as ~5.4 nm. The TEM image (Fig. 2) shows well dispersed Ni particles supported on support with an average diameter of 5.9 nm, agreeing well with the XRD result. Similar results were obtained with $LaCoO_3$ sample, except that the lanthanum species are mainly composed of $La(OH)_3$. Compared with $LaNiO_3$ and $LaCoO_3$, $LaFeO_3$ and $LaMnO_3$ samples remained their perovskite structures well after the reduction, because there is no obvious change on the diffractograms before and after the reduction, except that some weak diffraction peaks of La_2O_3 (JCPDS 050602) can be observed in the diffractogram of reduced $LaFeO_3$.

The fresh $LaNiO_3$, $LaCoO_3$, $LaFeO_3$, and $LaMnO_3$ samples were also tested by H_2-TPR, as shown in Fig. 3. $LaNiO_3$ shows two H_2 consumption peaks around 332 and 462 °C. They were originated from the reduction of $LaNiO_3$ to La_2NiO_5 and further to Ni^0, respectively [37,38]. Similar results were obtained over $LaCoO_3$, except that the two peaks are shifted to 327 and 487 °C. The TPR profiles of $LaFeO_3$ and $LaMnO_3$ show very weak hydrogen consumption, indicating that they are too stable to be reduced below 800 °C by H_2.

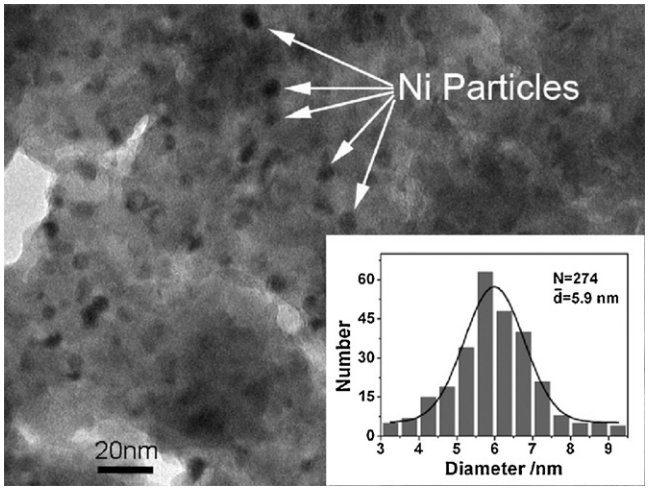

Fig. 2. TEM image of reduced $LaNiO_3$. The inset shows the histogram of the Ni particle diameter distribution.

Combining the XRD and TPR results, the reducibility of $LaNiO_3$, $LaCoO_3$, $LaFeO_3$ and $LaMnO_3$ perovskite samples is in the following order: $LaNiO_3 \approx LaCoO_3 > LaFeO_3 \approx LaMnO_3$. The order is well consistent with the order of the electronegativities of the center atoms (Ni: 1.91, Co: 1.88, Fe: 1.83, Mn: 1.55). In addition, the ionic radii of Ni and Co (60 and 61 pm) are much smaller than those of Mn and Fe (both 64.5 pm) [39], which highly agrees with the result on the reducibility.

The perovskite structures of $LaNiO_3$ and $LaCoO_3$ were destroyed totally by reduction, while the $LaMnO_3$ sample kept its structure well after reduction. It could be expected that the active centers of these perovskite-derived samples for ATRE reaction were different, thus the catalytic performance could be different. The features of active sites were characterized by EtOH-TPD experiments, as shown in Fig. 4. $LaNiO_3$ and $LaMnO_3$ were selected for a comparative study, since they are the representatives with highest and lowest reducibility. Ethanol desorption was not detected within the temperature range for the both samples, probably due to the higher desorption temperature employed [40]. The ethanol uptake on the reduced $LaNiO_3$ is about 71.5 μmol/g of catalyst. The ethanol absorbed dehydrogenates to form acetaldehyde over the reduced $LaNiO_3$ at quite low temperature of ~80 °C, as evidenced by a strong

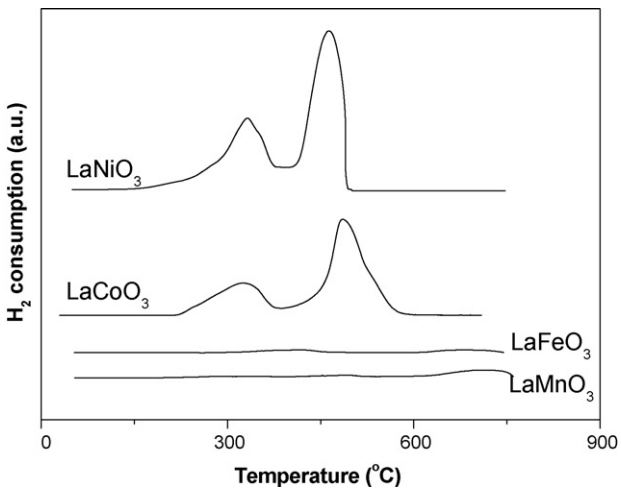

Fig. 3. H_2-TPR profiles of $LaNiO_3$, $LaCoO_3$, $LaFeO_3$ and $LaMnO_3$. Experimental conditions: 50 cm^3/min reductant (10 vol.% H_2 in Ar), 0.15 g catalyst, ramping rate 10 °C/min.

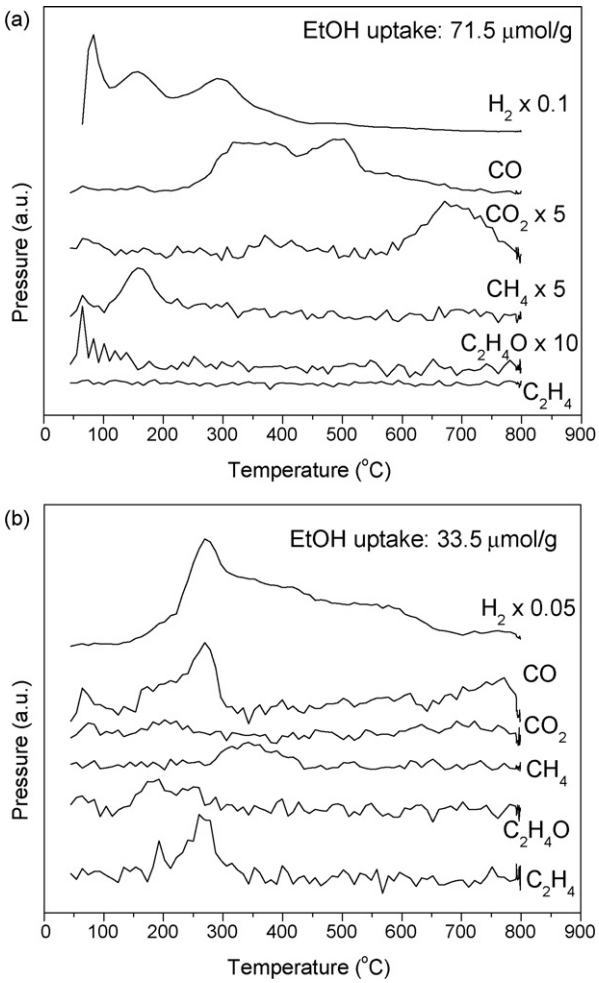

Fig. 4. EtOH-TPD profiles over reduced (a) $LaNiO_3$ and (b) $LaMnO_3$. Experimental conditions: 20 cm^3/min Ar, 0.10 g catalyst, ramping rate 10 °C/min.

H_2 peak and an acetaldehyde peak. Meanwhile, the decomposition of absorbed ethanol/acetaldehyde may also occur, as small amounts of CO and CH_4 were detected. When the temperature was increased to ~200 °C, the second H_2 peak was found associated with desorption of CH_4 and trace of CO, indicating the rupture of C–C bond. The decomposition of adsorbed acetaldehyde could also contribute to the production of methane. The third hydrogen peak appears at 200–400 °C, meanwhile a quite amount of CO and trace CH_4 are released, implying the decomposition of strongly adsorbed acetaldehyde/acetate [41,42]. CO_2 peak at ~700 °C can be attributed to the decomposition of lanthanum dioxycarbonate formed during the adsorption/decomposition of ethanol via the reaction: $La_2O_3 + CO_2 \leftrightarrow La_2O_2CO_3$ [40].

Compared with the reduced $LaNiO_3$, a much lower ethanol uptake of ~33.5 μmol/g of catalyst was detected over $LaMnO_3$ that remained the perovskite structure after reduction as demonstrated by XRD. A very broad hydrogen desorbed peak is ranged from 150 °C to 700 °C, and peaks at about 300 °C, indicating that the higher temperature is needed to extract hydrogen from ethanol over $LaMnO_3$ than that over $LaNiO_3$. It should be noted that a large amount of C_2H_4 was detected with the hydrogen peak, which is indicative of the dehydration reaction of ethanol and exposes the catalyst to the risk of coke deposition via the polymerization of C_2H_4 [43,44].

Above results suggest that the catalysts possess the activities for dehydrogenation of ethanol, C–C bond breaking/decomposition of acetaldehyde, and decomposition and reforming of adsorbed methane, through which hydrogen is generated. The facts that the dehydrogenation occurred at low temperature of ~80 °C, and that C–C bond cleavage occurred below 200 °C, indicate that the $LaNiO_3$ perovskite-derived catalyst may be an active one for hydrogen production. It will be demonstrated in the following section.

3.2. ATRE reaction performances over the perovskite-derived catalysts

Fig. 5 compares ATRE performances of the reduced $LaNiO_3$, $LaCoO_3$, $LaFeO_3$ and $LaMnO_3$ catalysts as a function of $EtOH/O_2$ ratio. All the catalysts showed considerable conversion efficiency higher than 80% in the ATRE reaction. Among these catalysts, the reduced $LaNiO_3$ exhibited the highest activity, while the $LaMnO_3$,

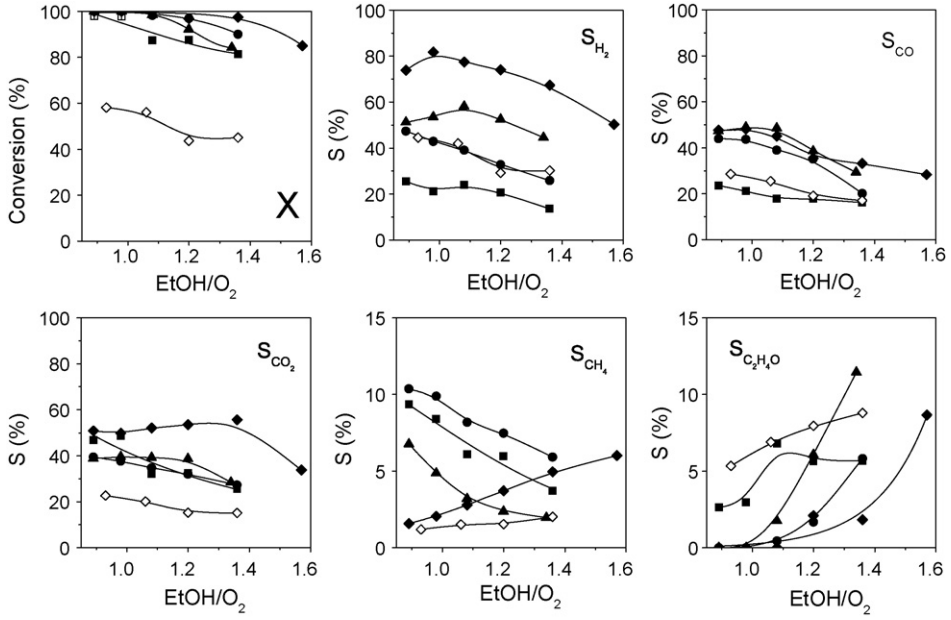

Fig. 5. ATRE reaction performances of reduced $LaNiO_3$, $LaCoO_3$, $LaFeO_3$, $LaMnO_3$ and unreduced $LaNiO_3$ catalysts. ATRE reaction conditions: $EtOH:H_2O = 1:2$, GHSV = $(2–4) \times 10^5$ h^{-1}, 1.5 h. $LaCoO_3$ (▲); $LaFeO_3$ (●); $LaMnO_3$ (■); reduced (♦) and unreduced (◊) $LaNiO_3$.

which remained the perovskite structure after reduction, was the most inactive one. To our knowledge, it is for the first time to report that perovskite oxides can catalyze ethanol reforming autothermally. Though the perovskite-derived catalysts can catalyze the ATRE reaction effectively, the product distributions differed from each other significantly. Depending on the catalyst used, the H_2 selectivity varied in a wide range from 20 to 80% with a rising order: $LaMnO_3 < LaFeO_3 < LaCoO_3 < LaNiO_3$. At $EtOH/O_2$ ratio of 0.98, Y_H^2 values, defined as moles of produced hydrogen per mole of ethanol, were 3.2 (water contributed to the formation of H_2), 2.1, 1.7 and 0.8 over $LaNiO_3$, $LaCoO_3$, $LaFeO_3$ and $LaMnO_3$, respectively. Except the high yield of H_2, the reduced $LaNiO_3$ also gave lower selectivities of methane and acetaldehyde, suggesting the higher activity for C–C bond cleavage and reforming reaction. The H_2 reduction played a crucial role in the activation of $LaNiO_3$. Over the unreduced $LaNiO_3$, very low conversions and H_2 selectivity were detected. Meanwhile, the selectivity of methane decreased and that of acetaldehyde increased, indicating that the unreduced $LaNiO_3$ is less active in C–C bond cleavage. Combining with the characterization results, these results suggest that the metallic nickel crystallites are needed for the hydrogen production.

Fig. 6 shows the bed temperatures as a function of $EtOH/O_2$ ratio. The bed temperature elevated from 400 to 500–720 °C, depending on the catalyst used, after the reactants were introduced into the reactor. At the same $EtOH/O_2$ ratio, the bed temperature was in the following rising order: $LaNiO_3 < LaCoO_3 < LaFeO_3 < LaMnO_3$. Under a thermal–neutral condition, the bed temperature related with the product distribution. The above temperature order is well consistent with the reverse one of H_2 yield. According to the characterization results, this order is also consistent with that of the extent on which the perovskite structure is destroyed. It suggests that the more serious total/partial oxidation that is highly exothermal is preferential on the refractory perovskite, rather than the reforming reaction to form H_2. This result agrees well with the features of selectivity patterns over various catalysts as aforementioned.

Above results demonstrated that the reduced $LaNiO_3$ catalyst showed superior performance in ATRE reaction to the other three catalysts. It could be due to the well dispersed Ni that favors the dehydrogenating and the breaking of C–C bond to produce hydrogen. Though the perovskite-type oxides also catalyze the ATRE reaction due to their high oxidative activity, they are not suitable for the production of hydrogen.

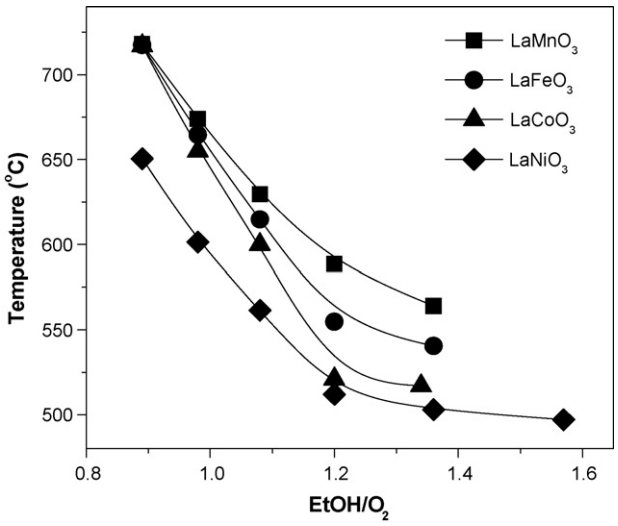

Fig. 6. The bed temperatures as a function of $EtOH/O_2$ ratio during the ATRE reaction over the reduced perovskite catalysts. ATRE reaction conditions: $EtOH:H_2O = 1:2$, GHSV = $(2–4) \times 10^5\ h^{-1}$, 1.5 h.

3.3. *Effect of preparing methods on the ATRE performances over Ni/La_2O_3*

Fig. 7 compares the ATRE performances as a function of $EtOH/O_2$ ratio over the Ni/La_2O_3 catalyst prepared by the impregnation method with the perovskite-derived one. For the convenience of comparison, the results of reduced $LaNiO_3$ in Fig. 5 are replotted. When the loading of Ni is same as $LaNiO_3$, namely 23.9 wt.%, the activity for the ATRE reaction of Ni/La_2O_3 is similar to the perovskite-derived one. However, the selectivity of H_2 is lower on $Ni(23.9)/La_2O_3$ than that on the perovskite-derived one. It is also noted that the C_2H_4O selectivity is higher on the impregnated catalyst, indicating lower activity for the C–C bond cleavage.

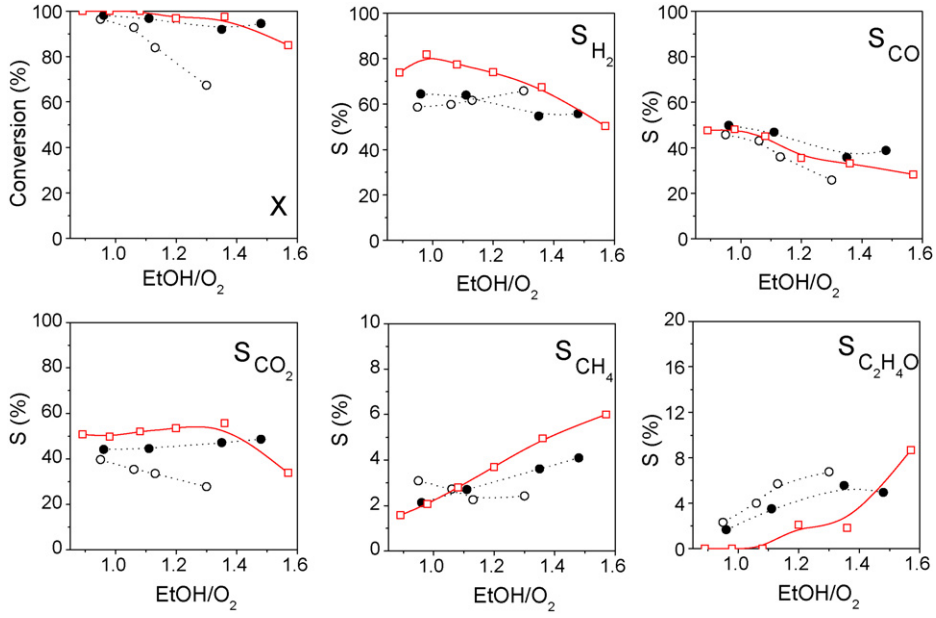

Fig. 7. ATRE reaction performances of $Ni(10)/La_2O_3$, $Ni(23.9)/La_2O_3$ and reduced $LaNiO_3$ catalysts. ATRE reaction conditions: $EtOH:H_2O = 1:2$, GHSV = $(2–4) \times 10^5\ h^{-1}$, 1.5 h. $Ni(10)/La_2O_3$-i (○); $Ni(23.9)/La_2O_3$-i (●); reduced $LaNiO_3$ (□).

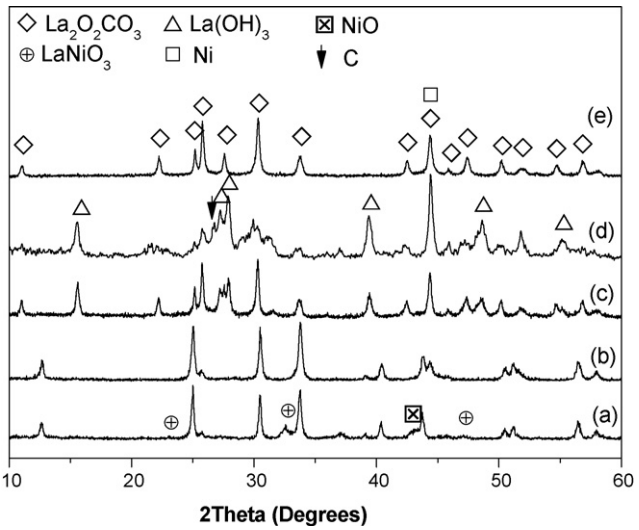

Fig. 8. XRD patterns of the as-prepared (a), reduced (b), used (c) Ni(10)/La_2O_3, used Ni(23.9)/La_2O_3 (d) and $LaNiO_3$ (e) catalysts. ATRE reaction conditions: EtOH:O_2:H_2O = 1:1.12:2, GHSV = 3×10^5 h^{-1} for 1.5 h.

Above result shows that the preparation method affects the ATRE performance significantly. For the production of hydrogen, the perovskite-derived nickel catalyst is preferred. Fig. 8 presents the diffraction patterns of Ni(10)/La_2O_3, Ni(23.9)/La_2O_3 and $LaNiO_3$ catalysts at various conditions. The fresh Ni(10)/La_2O_3 shows a group of diffraction peaks that can be attributed to lanthanum dioxycarbonate. The weak peaks at 32.5° and 43.4° can be assigned to $LaNiO_3$ (JCPDS 330711) and NiO (JCPDS 471049), respectively. After reducing the Ni(10)/La_2O_3 sample at 500 °C for 40 min, NiO and $LaNiO_3$ were converted into Ni^0, as evidenced by the diffraction peak at 44.5° (JCPDS 040850). Based on Scherrer's equation using the (1 0 0) reflection for both NiO and Ni, the particle sizes of NiO and Ni in the fresh and reduced Ni(10)/La_2O_3 samples are 8.9 and 18.2 nm, respectively, indicating the growth of Ni crystallites. After the ATRE reaction at EtOH/O_2 = 1:1.12 for 1.5 h, lanthanum oxide was partially converted into hexagonal $La_2O_2CO_3$ ($La_2O_2CO_3$-II). The absence of Ni could be due to the overlapping with the (1 1 0) reflection of $La_2O_2CO_3$-II at 2θ = 44.4° (JCPDS 370804). It should be noted that the (0 0 2) peak of graphitic carbon was detected in the used Ni(23.9)/La_2O_3. However, the carbon peak was absent in the perovskite-derived one. It is indicative of the more serious coke deposition over the impregnated catalyst. This can also be supported by the TEM analysis as shown in Fig. 9. The micrograph of used $LaNiO_3$ shows well dispersed Ni particles on $La_2O_2CO_3$.The Ni particles were in the range of 2 and 20 nm with an average size of 7.0 nm (Fig. 9(d)). No obvious coke was observed on $LaNiO_3$ after the reaction. However, on the impregnated Ni(10)/La_2O_3, Ni particles are in the range of 5–110 nm with an average size of 15.3 nm (see Fig. 9(b) and (e)). This size is much larger than that on $LaNiO_3$, indicating the sintering of Ni during the reaction. Over Ni(23.9)/La_2O_3, the Ni particle distribution is broadened to 10–120 nm, and the average size is 24.2 nm (see Fig. 9(c) and (f)). Moreover, abundant carbon filaments/nanotubes and graphitic carbon covering on Ni particles (the inset of Fig. 9(c)) are observed on the impregnated catalysts, indicating the serious deposition of coke. The deposition of carbon could be due to the much larger Ni particles according to the literature [18–21].

The comparison of ATRE reaction stability between the Ni(23.9)/La_2O_3 and the reduced $LaNiO_3$ catalysts is shown in Fig. 10. The reduced $LaNiO_3$ catalyst was stable within the time employed without any drop of conversion and H_2 selectivity. The average H_2 selectivity during 10 h was 71.0% for the reduced $LaNiO_3$. The Ni(23.9)/La_2O_3 catalyst showed an initial conversion of 94% and H_2 selectivity of 63%. It deactivated quickly with time on stream. After a 6 h ATRE reaction, the hydrogen selectivity dropped to 36.3%, a half of the initial one. Correspondingly, more CO, C_2H_4O and CH_4 were detected, indicating that the activities for C–C bond breaking, CH_4 reforming and WGS reaction decreased. This result is well consistent with the above-mentioned coking behaviors of these catalysts.

Above results demonstrate that the $LaNiO_3$ perovskite-derived Ni particles tend to disperse well on the $La_2O_2CO_3$ support, therefore improves the activity for the reactions involving C–C bond cleavage and the selectivity of hydrogen. Additionally, the ATRE stability and the resistance to coke deposition are also enhanced, because (1) the coke deposition rate strongly depends on the Ni particle size and the coking will be suppressed on the smaller Ni particles [18,21,45] and (2) the formation of $La_2O_2CO_3$ may also act as a carbon reservoir [46] through the reaction $La_2O_2CO_3 + C \rightarrow La_2O_3 + 2CO$. It is also shown that the sintering of Ni is suppressed deeply on the perovskite-derived sample. Rivas et al. [47] have reported that Ni nanocrystallites can be stabilized over $La_2O_2CO_3$, while aggregated over $La(OH)_3$. Our recent work [11]

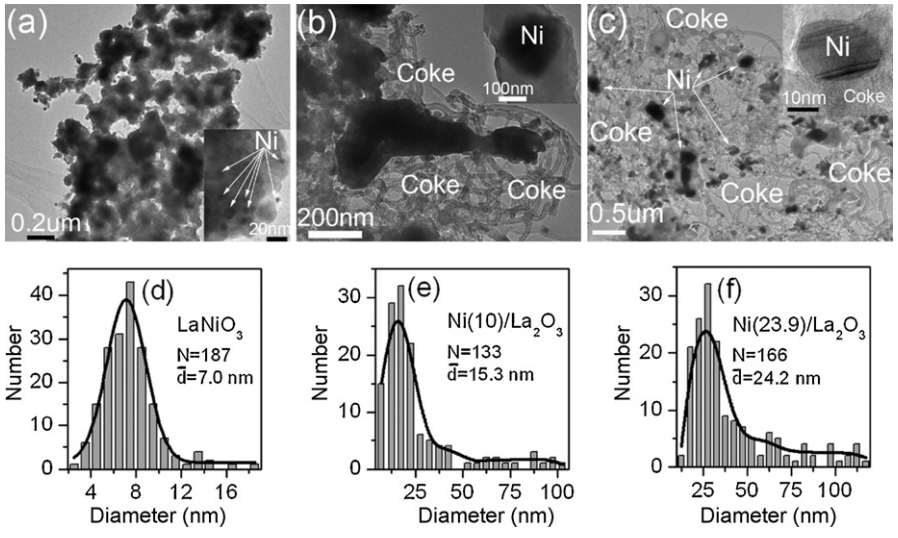

Fig. 9. TEM images of the used (a) $LaNiO_3$, (b) Ni(10)/La_2O_3 and (c) Ni(23.9)/La_2O_3 catalysts. The lower panels show the histograms of Ni particle diameter distribution of the used (d) $LaNiO_3$, (e) Ni(10)/La_2O_3 and (f) Ni(23.9)/La_2O_3 catalysts. ATRE reaction conditions: EtOH:O_2:H_2O = 1:1.12:2, GHSV = 3×10^5 h^{-1}, for 1.5 h.

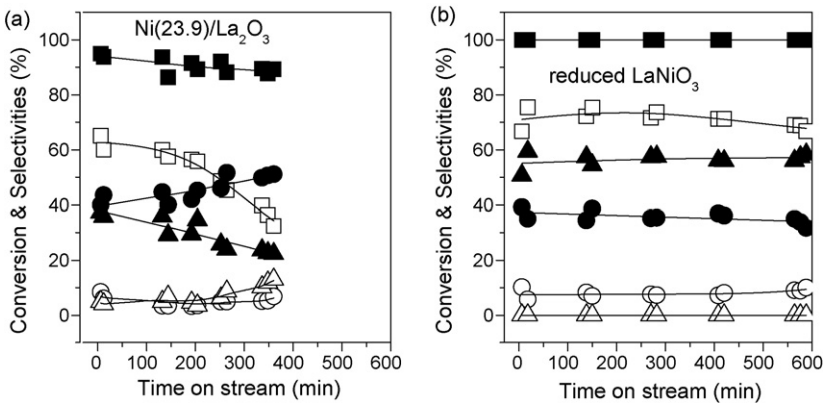

Fig. 10. ATRE reaction performances of (a) Ni(23.9)/La_2O_3 and (b) reduced $LaNiO_3$ catalysts as a function of time on stream. ATRE reaction conditions: EtOH:O_2:H_2O = 1:0.75:2 and GHSV = 3.5×10^5 h^{-1}. Conversion (■); selectivity of H_2 (□); CO (●); CH_4 (○); CO_2 (▲); and C_2H_4O (△).

shows that $La_2O_2CO_3$ strongly interacts with metal nanoparticles and suppresses the sintering by an *in situ* dispersion effect during the oxidative reforming reaction of ethanol. Hence, we speculate that the strong interaction between Ni and $La_2O_2CO_3$ may stabilize and decelerate the sintering of metallic nickel domains.

4. Conclusions

Perovskite-type $LaNiO_3$, $LaCoO_3$, $LaMnO_3$ and $LaFeO_3$ catalysts were prepared by the combustion method. After activating with H_2, the catalytic ATRE reaction was investigated over these catalysts. The reduced $LaNiO_3$ catalyst is highly active and selective for the ATRE reaction. Typically, 3.2 H_2 molecules per ethanol molecule were produced at EtOH:H_2O:O_2 = 1:2:0.98 and GHSV = 4×10^5 h^{-1}. Physicochemical characterizations show that well dispersed Ni is formed on lanthanum oxide support, which favors the dehydrogenation and decomposition of ethanol/acetaldehydes. Compared with the impregnated Ni/La_2O_3 catalyst, the perovskite-derived one is more active, stable and selective for hydrogen production. In addition, the coke deposition is suppressed significantly during the ATRE reaction compared with the impregnated one. It may be due to the formation of highly dispersed Ni nanoparticles from the perovskite precursor.

Acknowledgments

This work was supported by the National High Technology Research and Development Program of China (863 Program, No. 2009AA05Z102), the National Natural Science Foundation of China (No. 50675070) and the Fundamental Research Funds for the Central Universities of China (No. 2009zm0246).

References

[1] J. Dauenhauer, B.J. Dreyer, N.J. Degenstein, L.D. Schmidt, Angew. Chem. Int. Ed. 46 (2007) 5864.
[2] P.D. Vaidya, A.E. Rodrigues, Chem. Eng. J. 117 (2006) 39.
[3] P.R. de la Piscina, N. Homs, Chem. Soc. Rev. 37 (2008) 2459.
[4] M. Nilsson, X. Karatzas, B. Lindstrom, L.J. Pettersson, Chem. Eng. J. 142 (2008) 309.
[5] G.A. Deluga, J.R. Salge, L.D. Schmidt, X.E. Verykios, Science 303 (2004) 993.
[6] J.R. Salge, G.A. Deluga, L.D. Schmidt, J. Catal. 235 (2005) 69.
[7] R. Horn, K.A. Williams, N.J. Degenstein, A. Bitsch-Larsen, D.D. Nogare, S.A. Tupy, L.D. Schmidt, J. Catal. 249 (2007) 380.
[8] A.D. Qi, S.D. Wang, G.Z. Fu, C.J. Ni, D.Y. Wu, Appl. Catal. A: Gen. 281 (2005) 233.
[9] J.R. Mawdsley, T.R. Krause, Appl. Catal. A: Gen. 334 (2008) 311.
[10] H.Q. Chen, H. Yu, Y. Tang, M.Q. Pan, G.X. Yang, F. Peng, H.J. Wang, J. Yang, J. Nat. Gas Chem. 18 (2009) 191.
[11] H. Chen, H. Yu, F. Peng, H. Wang, J. Yang, M. Pan, J. Catal. 269 (2010) 281.
[12] D.K. Liguras, K. Goundani, X.E. Verykios, J. Power Sources 130 (2004) 30.
[13] M.C. Sanchez-Sanchez, R.M. Navarro, J.L.G. Fierro, Int. J. Hydrogen Energy 32 (2007) 1462.
[14] D.R. Sahoo, S. Vajpai, S. Patel, K.K. Pant, Chem. Eng. J. 125 (2007) 139.
[15] P. Biswas, D. Kunzru, Chem. Eng. J. 136 (2008) 41.
[16] E.B. Pereira, N. Homs, S. Marti, J.L.G. Fierro, P.R. de la Piscina, J. Catal. 257 (2008) 206.
[17] J. Llorca, N. Homs, J. Sales, J.L.G. Fierro, P.R. de la Piscina, J. Catal. 222 (2004) 470.
[18] A.J.H.M. Kock, P.K. de Bokx, E. Boellaard, W. Klop, J.W. Geus, J. Catal. 96 (1985) 468.
[19] D. Duprez, M.C. Demicheli, P. Marecot, J. Barbier, O.A. Ferretti, J. Catal. 124 (1990) 324.
[20] M.C. Demicheli, D. duprez, J. Barbier, O.A. Ferretti, E.N. Ponzi, J. Catal. 145 (1994) 437.
[21] S. Tang, L. Ji, J. Lin, H.C. Zeng, K.L. Tan, K. Li, J. Catal. 194 (2000) 424.
[22] A. Haryanto, S. Fernando, N. Murali, S. Adhikari, Energy Fuels 19 (2005) 2098.
[23] V.A. Tsipouriari, Z. Zhang, X.E. Verykios, J. Catal. 179 (1998) 283.
[24] Y. Cui, H. Zhang, H. Xu, W. Li, Appl. Catal. A: Gen. 331 (2007) 60.
[25] S.N. Pavlova, N.N. Sazonova, V.A. Sadykov, O.I. Snegurenko, V.A. Rogov, E.M. Moroz, I.A. Zolotarskii, A.V. Simakov, V.N. Parmon, Kinet. Catal. 45 (2004) 589.
[26] S.P. Jiang, J. Mater. Sci. 43 (2008) 6799.
[27] A.A. Bokov, Z.G. Ye, J. Mater. Sci. 41 (2006) 31.
[28] N. Labhsetwar, R.B. Biniwale, R. Kumar, S. Rayalu, S. Devotta, Catal. Surv. Asia 10 (2006) 55.
[29] M. Ni, M.K.H. Leung, D.Y.C. Leung, Int. J. Hydrogen Energy 33 (2008) 2337.
[30] S. Stolen, E. Bakken, C.E. Mohn, Phys. Chem. Chem. Phys. 8 (2006) 429.
[31] C. Batiot-Dupeyrat, G.A.S. Gallego, F. Mondragon, J. Barrault, J.M. Tatibouet, Catal. Today 107–108 (2005) 474.
[32] G. Valderrama, A. Kiennemann, M.R. Goldwasser, Catal. Today 133 (2008) 142.
[33] S.M. Lima, J.M. Assaf, M.A. Pena, J.L.G. Fierro, Appl. Catal. A: Gen. 311 (2006) 94.
[34] P. Dinka, A.S. Mukasyan, J. Power Sources 167 (2007) 472.
[35] G.S. Gallego, C. Batiot-Dupeyrat, J. Barrault, F. Mondragon, Ind. Eng. Chem. Res. 47 (2008) 9272.
[36] R. Pechini, US Patent 3,330,697 (1967).
[37] S.M. de Lima, M.A. Pena, J.L.G. Fierro, J.M. Assaf, Catal. Lett. 124 (2008) 195.
[38] S.M. de Lima, J.M. Assaf, Catal. Lett. 108 (2006) 63.
[39] J.A. Dean, Lange's Handbook of Chemistry, 15th ed., McGraw-Hill, New York, 1999.
[40] A.N. Fatsikostas, X.E. Verykios, J. Catal. 225 (2004) 439.
[41] L.V. Mattos, E. Noronha, J. Catal. 233 (2005) 453.
[42] E.M. Cordi, J.L. Falconer, J. Catal. 162 (1996) 104.
[43] M. Benito, J.L. Sanz, R. Isabel, R. Padilla, R. Arjona, L. Daza, J. Power Sources 151 (2005) 11.
[44] D.L. Trimm, Catal. Today 37 (1997) 233.
[45] M.C. Sanchez-Sanchez, R.M. Navarro, J.L.G. Fierro, Catal. Today 129 (2007) 336.
[46] A.N. Fatsikostas, D.I. Kondarides, X.E. Verykios, Catal. Today 75 (2002) 145.
[47] M.E. Rivas, J.L.G. Fierro, M.R. Goldwasser, E. Pietri, M.J. Perez-Zurita, A. Griboval-Constant, G. Leclercq, Appl. Catal. A: Gen. 344 (2008) 10.